A ZERO-DIMENSIONAL MODEL TO SIMULATE INJECTION RATE FROM FIRST GENERATION COMMON RAIL DIESEL INJECTORS UNDER THERMODYNAMIC DIAGNOSIS

Soriano, J.A.[1]; Mata, C.[2*]; Armas, O.[1]; Ávila, C.[3]

1. Universidad de Castilla-La Mancha. Campus de Excelencia Internacional en Energía y Medioambiente. Escuela de Ingeniería Industrial de Toledo, Real Fábrica de Armas. Edif. Sabatini. Av. Carlos III, s/n. 45071 Toledo, Spain.

2. Universidad de Castilla-La Mancha. Campus de Excelencia Internacional en Energía y Medioambiente. Escuela de Ingeniería Minera e Industrial de Almadén, Plaza Manuel Meca s/n. 13400 Almadén, Spain.

3. Department of Mechanical Engineering, Universidad de Antioquia, Calle 70 No. 52-21, Medellín, Colombia.

** Corresponding author: maricarmen.mata@uclm.es*

ABSTRACT

The injection rate curve is an important input parameter in the thermodynamic diagnosis and in the predictive models, and it can also be used to simulate fuel sprays under different operating conditions. In this work, a zero-dimensional fuel injection rate model is proposed from experimental data obtained from a common-rail injection system with two solenoid-operated injectors. The model proposed is a useful tool when the internal component's dimensions of the injector are unknown. The presented model only requires the injection pressure, the injector energization signal, the total fuel mass consumed per stroke, the geometry and the holes number of the fuel injector and, finally, some physical properties of fuel. The model has been applied to two different solenoid-operated injectors and two fuels. The comparative results between the experimental and the modelled fuel injection rate show excellent results despite the simplicity of the experimental data requirements. The effects of the introduction of the modelled and measured fuel injection rate in a thermodynamic diagnostic tool are shown. This proposed model can be a useful, simple and alternative tool for estimating rates of injection without the need to carry out a test of the rate of injection.

Keywords: *Diesel injection, solenoid-operated injector, fuel injection modelling, thermodynamic diagnosis, zero-dimensional model, GTL fuel.*

1. INTRODUCTION

Nowadays, the well-known common-rail injection technology achieves better results than the traditional injection system due to higher flexibility for all load ranges. This system makes possible to regulate the injection parameters (such as the start and duration of injections and the injection pressure) with high precision at any operating mode of the engines. Moreover, the study of the rate of fuel injection (RoI) allows controlling the rate of heat release (RoHR) characteristics. In consequence, the fuel injection rate optimization is directly related to the in-cylinder combustion process.

Current injection strategies are characterized by short injection times and more than one injection per cylinder and cycle. Several studies have researched the effects of different injection strategies [1, 2]. Normally, these studies require a dedicated and complex facility apart from the engine test bench (where it is difficult to measure the real rate of injection accurately). However, if this research facility is not available, it would be helpful to have a model that is able to provide the rate signal from some known performance parameters (such as injector geometry, the pulse of energization, injection pressure, etc.). The existing literature about models for simulation of the rate is wide, but the premises for the development of the model are not always the same.

Most of the researchers working on fuel injection rate simulation focus on the hydraulic one-dimensional modelling (1D) of the injector, which requires a thorough knowledge of the dimensions and operation conditions of the injector. For the modelling the injector components, researchers have used computational tools such as AMESim code [3] or other similar software. Usually, these models are divided according to the injector type used: solenoid [4-8] or piezoelectric [9-11]. Solenoid operated injectors (the most used in last decade) have been studied and reported in several works. Seykens *et al.* [5], using an 8-hole injector, modeled the needle displacement caused by injection pressure variation which produced different slopes in the fuel injection rate. Chung et al. [6] modeled the rate of injection from the study of fuel flow through the injector and the forces involved during

the injection process. In this paper, a single injector outlet is used in the nozzle and, a single rate is simulated. Payri *et al.* [4], modeled a 6-hole solenoid injector and took into account the effects of the discharge coefficient and cavitation on the nozzle. Marcic *et al*. [8] used a 6-hole solenoid injector for the development of a needle movement dynamic model to simulate multiple injection rates. The most important disadvantages of these models are the need of accurately knowing the internal dimension of injectors.

In order to avoid this issue, Payri *et al.* [12] developed a zero-dimensional model (0D) assuming the injector as a black box, and directly calculating the rate of injection signal as a function of some easy to know geometrical and operating parameters, and the mathematical equations of the fluid-dynamic study at the nozzle outlet. This work is an example the use of 0D models, to reduce calculation time.

The use of injection models to simulate the effect of properties of alternative fuels to diesel is not overly usual [5, 7, 9, 11, 13]. This type of models has equations to estimate fuel properties (density, kinematic viscosity or bulk modulus) or experimental data [7, 9] necessary to use the models.

Different parameters such as injector type, test conditions or fuel properties may affect the results provided by the model. Although the possible differences (concerning real values) are low, they should be considered when fuel mass rate modelled is used to calculate heat release rate. In this sense, the thermodynamic diagnosis helps to understand the importance of these parameters during combustion [13-16].

The present work proposes a zero-dimensional model, which allows obtaining the rate of fuel injection, knowing the injection pressure, the injector energizing time, the total mass injected in each injection, the injection temperature, characteristics of the injector nozzle (diameter and number of holes), the gap between the start of injections (in case of multi-injection) and some fuel properties. Compared to other models, the model presented is able to simulate both single injection and split injection (pre-injection and main injection), in current engine operation modes or other unusual modes. For the development of the model, the experimental results of two solenoid injectors, with a different number of holes, were used. The stated model works with conventional diesel fuel without biodiesel and Gas To Liquid fuel (GTL). Fuel properties, such as density and viscosity, are determined by means of correlations as a function of fuel temperature and pressure. Finally,

the effect of the fuel introduction in the combustion chamber has been studied comparing two situations: i) with vs without fuel introduction and ii) modelled and measured injection rates, on the gas properties, in-cylinder mean temperature and heat release law are the main results of the thermodynamic diagnosis presented.

2. EXPERIMENTAL SETUP AND TEST PROCEDURE

2.1. Experimental installation and injectors tested

Figure 1 shows the experimental installation used for determination of the rate of fuel injection. The complete installation is described by Armas *et al.* [17].

Figure 1. Simple functional scheme experimental installation.

The experimental fuel injection rates were measured by means of fuel injection rate indicator IAV model EVI2 K-050-49 (IRI).

The signal of injector energizing was registered by means of an AC/DC Current Clamp, Hantek® CC 65, 20kHz bandwidth, (±2% of error in the range used), while the total fuel mass injected (m_f) was measured by a gravimetric balance KERN PFB 3000-2 with a precision of ±0,01g. Two different solenoid operated injectors have been used in this work: a) a 7-hole injector with 150 μm diameter (Denso model 7H150) and b) an 8-hole injector with 138 μm diameter (Denso model 8H138). Both injectors were used for developing the model approach and also for its validation under different operating modes. The operating parameters of the injectors were for the boost current 20 A and 75 V, and for the hold current 17 A and 13 V. In these injectors, the needle raising conditions cannot be varied, nor can it make boot and ramp shaped main injections.

The nozzle geometry was identified by means of an X-ray scanner NIKON model CT-SCAN-XT-H-160. The software of the scanner generates tridimensional (3D) images of the object from two-dimensional images (2D). Figure 2 shows an example of the images used to determine the nozzle diameter.

Figure 2. An example of the image from the tip of injector obtained by means X-ray analysis.

In this work, it is also used a test bench equipped with the light-duty engine NISSAN YD22, with 7H150 injectors. This installation is described by Payo *et al.* [18]. The main characteristics of the engine are shown in Table 1.

Table 1. Engine characteristics

2.2. Test fuels

2.2.1. Fuel properties

The development of the model and its application (with both injectors), were done using neat diesel fuel (without biodiesel). The model contemplates the possibility to work with a GTL fuel. This alternative fuel, obtained from natural gas or from renewable sources (biomass gasification) through a Fischer-Tropsch process, presents great potential to be used in diesel engines [19]. The diesel fuel was supplied by REPSOL Co. while the GTL fuel was supplied by SASOL Co. Table 2 shows the main properties of both fuels.

Table 2 Fuel properties

The atmospheric pressure experimental data for fuel density and kinematic viscosity are presented in Table 3.

Table 3. Kinematic viscosity and density of fuels tested at different temperatures with atmospheric pressure

2.2.2. Fuel density estimation

The fuel density (ρ_f) and kinematic viscosity (ν_f) oscillate with temperature and pressure.

Equation 1, proposed by Payri *et al.* [20], determines the diesel fuel density as a function of pressure and temperature, the reference temperature (T_0) is 313 K, and the reference pressure (P_0) is 0.1 MPa. The back temperature of injector fuel return is T and injection pressure is P. The ranges of applicability for this expression are 298K to 348K in temperature and 0.1MPa to 180MPa in pressure.

$$\rho(P,T) = 835.698 - 0.628(T - T_0) + 0.491(P - P_0) - 0.00070499(T - T_0)^2 + 0.00073739(P - P_0)^2 + 0.00103633(P - P_0)(T - T_0) \quad (1)$$

Outcalt *et al.* [21] used the expression (2) to determine the density of GTL fuel as a function of pressure and temperature. For this expression, is needed a GTL fuel density correlation, depending on temperature, at the reference pressure (applicability 270K to 470K in temperature and 0.48MPa to 50MPa in pressure).

$$\rho(P,T) = \frac{\rho(P_0,T)}{1 - 0.082681 \cdot \ln\left(\frac{P + B(T)}{P_0 + B(T)}\right)} \quad (2)$$

For calculating $\rho(P_0,T)$, the equation proposed by Rackett [22] and the experimental data presented in Table 3 was used.

$$\rho(P_0,T) = 255.5 \cdot 0.519^{-(1+(1-T/578.2)^{0.542})} \quad (3)$$

Where *B(T)* is Tait equation parameter defined by Dymond and Malhotra [23], which can be expressed by the equation (4).

$$B(T) = 325.49 - 298.96\,T/273 + 70.73(T/273)^2 \quad (4)$$

2.2.3 Fuel dynamic viscosity estimation

The fuel density and the fuel dynamic viscosity depends on pressure and temperature. From the experimental data shown in Table 3, exponential expressions (5) and (6) were obtained to define the dependence of the dynamic viscosity (μ_f) with the temperature, at a reference pressure and for each fuel, such as those presented by Payri *et al.* [24].

$$\mu_{Diesel}(P_0,T) = 5.7694e^{-0.0169T} \quad (5)$$

$$\mu_{GTL}(P_0,T) = 4.7883e^{-0.0189T} \quad (6)$$

In the expressions (5) and (6) the fuel dynamic viscosity is given in cPo while the fuel temperature is given in ºC.

For calculating the dynamic viscosity variation caused by the fuel pressure, expression (5) and (6) are replaced by the expression (7), proposed by Kousel [25].

$$\mu_f(P,T) = \mu_f(P_0,T)\exp\left[\frac{P}{10^4}\left(7.9718 + 37.27967\mu_f(P_0,T)^{0.278}\right)\right] \quad (7)$$

2.3. Test plan

In this work, rates of fuel injections from two different test plans were used:

i) A test plan with an injector denoted as 7H150, previously mounted in an engine coupled to a dynamometer in a test bench.

ii) A test plan with a similar injector denoted as 8H138, used for determining its discharge coefficient.

Originally, the first test plan was used in order to experimentally characterize exhaust pipe heat transfer of the engine [26]. The main advantage of using these two test plans consists of the possibility to test the injectors with multiple injections with short energizing times, characteristic of both urban and extra-urban driving conditions (test plan i), and with long injector energizing time as employed typically of used in a test for spray modelling (test plan ii). Different operating modes from each test plan were used for model approach and its validation.

Table 4 shows the characteristic injection parameters of the test plan used for the model approach (modes with asterisks) and its validation (modes without asterisks), using the 7H150 injector and the experimental installation shown in Figure 1. Values of injection pressure and injection timing shown in Table 4 were recorded from tests carried out in the test bench with the light-duty engine NISSAN YD22, equipped with 7H150 injector. Figure 3 shows these engine operating modes [26].

Table 4 Main characteristic parameters of injection for split injection with Denso 7H150 injector (9 engine modes).

As can be seen in Figure 3, the 9 operating modes are located in the lower-left zone of the engine map (Torque-engine speed), limited by the full load curve (maximum torque at each engine speed). These modes cover the most part of the zone characterized by the New European Driving Cycle (NEDC) [26].

The outermost modes (A, C, G, and I) and the central mode (E) were selected for the model approach, while the parameters from modes B, D, F, and H were used for model validation. All modes used have two injections (pre-injection and main injection) and were tested in the installation presented in Figure 1 using two different dwell times (time between injections) at each operating mode.

Figure 3. Engine operating modes used for 0D model input data with 7H150 injector.

Table 5 shows the injection characteristic parameters of the nine modes for calculating RoI related to the second injector Denso 8H138. Six of them for the model development (denoted with an additional asterisk) and three used for the model validation.

Table 5. Main injection characteristic parameters for single injection using Denso 8H138 injector.

2.4. Methodology

During all the tests for determining rates of fuel injection (Tables 4 and 5), the fuel temperature at the inlet of the high-pressure pump was constant (around 40ºC). The return back pressure (P_{rp}) of injectors was 0.975 bar in all cases and injectors. The methodology presented in this paper was divided into three parts:

- General methodology for the model approach (Figure 4).
- Model validation with different fuels (Figure 5).
- Model application and validation across the thermodynamic diagnosis (Figure 6).

Figure 4 shows the methodology used for the model approach. Using geometrical data from both injectors, experimental data from IRI (RoI and energizing signals, and mass injected for each injection) and fuel properties (in this case, density and dynamic viscosity diesel fuel equations) the different characteristic parameters of the model were determined and developed. Experimental data includes values from 11 different operating modes tested

with diesel fuel, 5 split injections (pre + main injections) with 7H150 injector and 6 modes only with a main injection with the 8H138 injector. After model approach, modelled and experimental values of the rates of injections were compared.

Figure 4 Methodology for model approach.

To validate the model, (as shown in figure 5) two sets of data were used:

- Results obtained with diesel fuel (route with arrows and boxes drawn in continuous lines) under stationary modes B, D, F and H of Table 4 with injector 7H150 and modes 3, 6 and 9 of Table 5 with injector 8H138.
- Results obtained with GTL fuel (route with arrows and boxes drawn in dashed lines) in order to verify the ability of the model to reproduce rate of injections with different fuels, under operating modes A, C, G, I and E with injector 7H150 which appear in Table 4.

All modeled results were compared with the experimental data from the IRI and each fuel.

Figure 5 Methodology for model approach and its validation with different fuels.

Figure 6 shows the methodology followed to compare modelled and experimental rates of injections applied to a thermodynamic diagnosis model with both Diesel and GTL fuels and 7H150 injector. Experimental and modelled rates of injection were used as input data to the thermodynamic diagnostic model and are based on the estimation of thermodynamic properties of the gas, derived from the experimental pressure signal in the cylinder [27] and improved by Payri *et al.* [14]. It allows obtaining comparative results of the in-cylinder gas mean temperature, RoHR and Heat Release Law (HRL). The comparison of results with the experimental RoI, the modeled RoI and without the RoI, allows the evaluations of the influence of the injection rate on the thermodynamic diagnosis.

Figure 6 Methodology to compare thermodynamic diagnosis results

3. MODEL PROPOSAL

Figure 7 shows an example of simple injection for an energizing time (*ET*) of the injector and its corresponding curve of rate of injection versus time. The injection time (t_{inj}) is obtained by means of the equation 8 which depends on: i) the energizing time of injector, ii) the time lag (d_1) between the start of the energizing (*SoE*) and the start of the injection (*SoI*) and iii) the time lag (d_2) between the end of the energizing (*EoE*) and the end of the injection (*EoI*).

$$t_{inj} = ET - d_1 + d_2 \tag{8}$$

When the injector works under single injection, the time lags d_1 and d_2 depend on the injector type, the injection pressure and the fuel used [17]. However, when the injector works under split injection, these time lags could be influenced by the time between injections or dwell time (D_T) [28], defined as the time between the end of the previous injection and the beginning of the next injection during the same thermodynamic cycle. In this proposal, the model takes into account this variation. For this reason, the calculated correlations include D_T as a factor in the correlation for determining d_1.

Taking into account the data collected from the two injectors under study, the equations 9 and 10 are proposed. The determination of the delay time d_1 is based on a correlation which takes into account: injection pressure and back pressure in return line of the injector (P_{inj} and P_{rp}, respectively), fuel density and dynamic viscosity (μ_f), and D_T. In the specialized literature, most of the studies use the Reynolds number (Re) for estimating both d_1 and d_2 delays. In this work have been taken into account some physical parameters that affect Re determination, but not its value. Correlation includes the effect of D_T on d_1 and the effect of ET on d_2, as it is done in other studies [12].

$$d_1 \approx a_1 + a_2\sqrt{P_{inj} - P_{rp}} + a_3\left(\frac{\sqrt{2\rho_f}}{\mu_f}\right)^2 + a_4\frac{\sqrt{2\rho_f}}{\mu_f} + a_5 D_T \tag{9}$$

The d_1 values remain practically constant (around 0.43 – 0.47ms), independently of the injector and the operating parameters. The maximum error of d_1 predicted value is

0.05ms, the average absolute error was 0.00193 ms and the R-squared was 99.93 %. Since the P-value, in Table 6, is less than 0.05, there is a statistically significant relationship between the variables with a confidence level of 95.0 %.

Related to the d_2 determination, a correlation is proposed (Equation 10). This correlation includes the effect of the following parameters: the number of nozzle orifices (z_0) and its diameter (d_0) of injectors, energizing time, injection pressure and the back pressure downstream of the injector. The maximum error of d_2 predicted value is 0.217ms in the longest energizations (2.5ms). The average absolute error was 0.02848 ms and the R-squared was 99.40 %. Since the P-value in Table 6 is less than 0.05, there is a statistically significant relationship between the variables with a confidence level of 95.0 %.

$$d_2 \approx b_1 + b_2\sqrt{P_{inj} - P_{back}} + b_3\frac{d_0}{z_0} + b_4 ET \qquad (10)$$

Values of the coefficients used in both correlations, are shown in Table 6.

Table 6. Coefficient of d_1 and d_2 correlation.

To obtain the modelled fuel injection rate closer to the experimental one and since the rate shape affects the spray penetration [29], it is necessary to take into account that the actual rate signal is composed of three zones (Figure 7): i) first part of the rate with positive slope; ii) second part, quasi-stationary rate with an almost constant value, and iii) third part, rate with negative slope. The positive and negative slopes depend on the injection pressure and the governing mechanism of the needle injector movement [20-25, 27, 30] for the same fuel. Additionally, the use of different fuels could affect the slope and the maximum level that reaches the rate at quasi-stationary zone [15].

Figure 7. Experimental actual event of fuel injection process.

For reproducing the slopes of the modelled rates of injection curves during their increase (or decrease), data registered during the tests detailed in Tables 4 and 5 were used. In order to simplify the model, a similar correlation was used for up and down slopes (with

positive or negative denotation). For reproducing the decrease of the rate of injection curves, was used the same but with a negative sign.

The correlations for determining positive and negative slopes are presented in equations 11 and 12, and their coefficients are presented in Table 7. The average absolute error was 0.0922486 and the R-squared was 76.16 %. Since the P-value in Table 7 is less than 0.05, there is a statistically significant relationship between the variables with a confidence level of 95.0 %.

$$Slope^{+} \approx c_1 + c_2\sqrt{P_{inj} - P_{back}} + c_3\frac{d_0}{z_0} \quad (11)$$

$$Slope^{-} \approx -c_1 - c_2\sqrt{P_{inj} - P_{back}} - c_3\frac{d_0}{z_0} \quad (12)$$

Table 7. Coefficients of correlation for determination of positive and negative slopes.

With the combination of the curves generated by both slope correlations (positive and negative), a triangular rate of injection (TRI) is obtained as Figure 8 shows. The maximum value of the experimental rate of injection signal is established by equation 13.

$$\dot{m}_f = C_d A_o \sqrt{2\rho_f (P_{inj} - P_{back})} \quad (13)$$

Where C_d is the injector nozzle discharge coefficient, A_o is the total injection discharge section area, ρ_f is the fuel density, P_{back} is the back pressure inside the fuel indicator, and P_{inj} is the injection Pressure.

The closed area of the TRI may not match with the total mass injected measured under the experimental test. Then, the model uses the total mass injected under the test to achieve the rate of injection shape as follows:

- When the total mass obtained from TRI is less than the experimental value, the model increases the slopes until matching both modelled and experimental injected total mass. In this case, the modelled RoI is always triangular.

- When the total mass obtained from TRI is higher than the experimental value, the model calculates a RoI using the slope correlations. However, the maximum value that the modelled RoI can reach is limited by the maximum delivery for each pressure. The value of maximum delivery for each pressure was calculated using the equation 13. The slopes can be increased (until the mass corresponding to the modelled rate coincides with the experimental mass), to avoid that the modelled RoI never surpasses the maximum value.

For refining the coincidence between modelled and measured values under trapezoidal RoI, the model smoothes the transition between the straight lines of the slopes and the rate limit as Figure 8 shows.

Figure 8. Simple modelled rates of fuel injection vs experimental rate.

In the case of multiple injections, the model is capable of distributing the total mass injected in each cycle, depending on the energization signal to obtain the mass of each injection, before beginning the process of modeling the signal.

4. RESULTS AND DISCUSSION

4.1. Comparison between modelled and experimental rates of injection.

For a better comprehension of results obtained in this work, this section has been divided into four sub-sections following the same order of the Figures 4, 5 and 6.

Figure 9 shows, as an example, the comparison between the modelled and the experimental RoI with injector 7H150 from the four operating modes used for the model validation (B, D, F and H modes). Results show that the model is able to reproduce the shape and the quantity of fuel injected under split injection processes. The maximum shot to shot difference between the modelled and the experimental RoI is 31 % and was observed in F modes. However, the maximum cycle to cycle difference is lower than 1 % and it decreases with the injected mass increase.

Figure 9. Modelled and experimental rates of injection. Operating modes B, D, F and H, were used for model validation.

4.2. Model application using the injector 8H138.

Figure 10 presents results from 8H138 solenoid-operated injector in order to check the model ability to reproduce rates of injection produced by another injector.

Figure 10. Modelled and experimental rates of injection. Operating modes 3, 6 and 9, used for model validation of the injector 8H138.

In this case, experimental modes used for comparison were 3, 6 and 9 (See Table 5). Modelled and experimental results obtained show that shot to shot differences are greater than in the case of the 7H150 injector. However, cycle to cycle differences are lower than 0.5 %.

Summarizing, the cycle to cycle differences between modelled and experimental RoI are acceptable while shot to shot differences could be questionable depending on the final use of modelled RoI.

4.3. Model application using GTL fuel and the injector 7H150.

In order to demonstrate the capability of the model with different fuel, similar tests to those presented in Figure 9, were carried out with GTL fuel in 5 modes (modes used to approach the model with diesel). Figure 11 shows that the model reproduces the RoI with GTL fuel with similar trends as to when Diesel fuel was tested.

Figure 11. Modelled and experimental rates of injection. Operating modes A, E and I, used for model approach and GTL fuel.

4.4. Application to thermodynamic diagnosis

As presented in Figure 6, modelled and experimental rates of injection were used as input data in a zero-dimensional thermodynamic model in order to obtain comparative results of the in-cylinder gas mean temperature and both the rate of heat release (RoHR) and the heat release law (HRL). In the thermodynamic model used, the in-cylinder instantaneous mean temperature of the gas (T_i) is calculated using the known gas state equation 14:

$$\frac{p_i V_i}{m_i R_i} = T_i \qquad (14)$$

Where p_i is the in-cylinder gas pressure, V_i is the in-cylinder calculated volume, m_i is the instantaneous in-cylinder trapped mass, R_i is the instantaneous specific constant of the In-cylinder gas.

The thermodynamic model works with three species: intake air, evaporated fuel and stoichiometric burnt products [14, 27]. The introduction of the evaporated fuel as specie, has two direct effects on the T_i: i) in-cylinder mass will change along the injection process and ii) R_i will change along the thermodynamic cycle according to the evolution of the mass fractions (Y_{xi}) of the mentioned species as equation 15 shows.

$$R_i = R_a\, Y_{ai} + R_f\, Y_{fi} + R_b\, Y_{bi} \qquad (15)$$

Where R_a is the specific air constant, R_f is the specific constant of the evaporated fuel and both are constant values [27] while R_b (specific constant of burnt products) depends on the temperature of the products as can be seen in Figure 12.

This result was obtained by means of a model which calculates the composition of the burnt products from a reaction with stoichiometric fuel-air ratio and, in consequence, the relative fuel-air ratio Fr = 1 with air and a diesel fuel with a mean molecular composition $C_{10.8}\ H_{18.7}$. The model used was adapted from the proposed model by *Way* [31]. The model considers 12 chemical species (including dissociation products) and establishes 5 atomic balances and 7 characteristic equilibrium reactions.

Figure 12. Variation of the specific constant of stoichiometric burnt products [32].

Variations of the gas constant of the burnt products with temperature are significant when it is high enough for dissociation to occur, which leads to the appearance of monoatomic species, with low molecular weight. However, as the T_i is never high enough to expect a significant increase in the gas constant, it is acceptable to adopt a fixed value for this constant, as for air and fuel (equation 16).

$$R_f = \frac{R_\mu}{MW_f} = 55.95\, J/kgK$$

$$R_a = \frac{R_\mu}{MW_a} = 287\, J/kgK \quad (16)$$

$$R_b = \frac{R_\mu}{MW_b} = 285.4\, J/kgK$$

Where MW_f, MW_a, MW_b are molecular weights of fuel, air, and burnt products, respectively, and Rμ is the universal constant.

Figure 13 shows, as an example, the evolution of the air, evaporated fuel and burnt products mass fractions as a function of crank angle under a combustion engine with the experimental rate of fuel injection test and under a combustion engine without the RoI. In this case, the test was carried out with split injection.

Figure 13. Evolution of the air, evaporated fuel and stoichiometric burnt products mass fractions a) under a combustion engine without the rate of fuel injection and b) under a combustion engine with a split rate of fuel injection.

Figure 14 shows the angle evolution of the R_i calculated with and without taking into account the introduction of fuel into the combustion chamber of the engine, using the same data of the test presented in Figure 13.

Figure 14 Evolution specific constant of the in-cylinder gas with split injection.

As can be seen in Figure 15, the instantaneous R_i reduction does not produce a decrease of the calculated T_i because of the effect of the increase of the in-cylinder mass is higher than the reduction of the R_i on the calculated gas temperature.

Figure 15 Evolution of the in-cylinder gas mean temperature with split injection.

The effect of introducing the rate of injection as input data in the thermodynamic diagnosis has been evaluated in three possible scenarios (using the experimental RoI, the

modelled RoI and without the RoI), in order to evaluate the differences produced on T_i, RoHR, and HRL.

Figure 16 shows (from top to the bottom) the RoI curves (modelled and experimental) and the in-cylinder pressure signal (input file for the diagnostic model). Also, the T_i, the RoHR, and the HRL versus crank angle were calculated with the RoI (modelled and experimental) and without the RoI, as thermodynamic diagnosis results, from the operating mode I with diesel fuel as an example. Values of T_i calculated without the RoI are higher than those obtained considering the RoI (modelled and experimental), as it was shown in Figure 15.

The thermodynamic model used in this work calculates the RoHR by means of the equation 17 [27]:

$$\mathrm{m}_i \mathrm{du}_i + \left(\mathrm{u}_b - \frac{u_f \left(\frac{f}{a}\right)_{st} + u_a}{\left(\frac{f}{a}\right)_{st} + 1} \right) (\mathrm{dm_b} + \mathrm{Y_b dm_{bb}}) =$$

$$-p_i \mathrm{d}V_i - \mathrm{d}Q_\mathrm{w} + \left(\mathrm{h_{finj}} - \mathrm{u_f}\right)\mathrm{dm_{fev}} - \mathrm{R_i T}_i \mathrm{dm_{bb}} \qquad (17)$$

Where u_i is the internal energy of the in-cylinder trapped mass, u_b is the internal energy of the stoichiometric burnt products, u_f is the internal energy of evaporated fuel, $\left(\frac{f}{a}\right)_{st}$ is the stoichiometric fuel to air ratio, u_a is the internal energy of the inlet air, $\mathrm{m_b}$ is the mass of stoichiometric burnt products, $\mathrm{Y_b}$ is the stoichiometric mass fraction of the burnt products, $\mathrm{m_{bb}}$ is the mass of blow-by, Q_w is the heat transferred to cylinder walls, $\mathrm{h_{finj}}$ is the enthalpy of fuel under the injection and $\mathrm{m_{fev}}$ is the mass of the evaporated fuel.

Values of the RoHR were calculated using the equation 17 (left term of the equation). Curves related to this parameter, and their cumulative values (HRL), were lower when the RoI is not taken into account since equation 17 is solved without the effect of the fuel introduction as a specie in the thermodynamic model.

Also, Figure 16 shows that the thermodynamic model results with the modelled and experimental RoI have reasonable accuracy. The shot to shot and cycle to cycle differences

between modelled and experimental rates of injection are acceptable for their use in thermodynamic diagnosis.

Figure 16. Thermodynamic diagnosis of the combustion process with diesel fuel from operating mode I.

Results presented confirmed that the use of the proposed model for estimating the rates of injection, as input data in thermodynamic diagnosis under different engine operating modes and fuels, has high accuracy when determining the $\boldsymbol{T_i}$, the RoHR, and the HRL compared to the thermodynamic diagnosis with the experimental RoI used as input data. These results also confirm the possibility to use this empirical, simple but also a robust zero-dimensional model for calculating instantaneous introduction of fuel in the combustion chamber as a species together with air and burnt products along the thermodynamic cycle.

6. CONCLUSIONS

In this work, empirical, simple and robust correlations for determining the delay time between SoE and SoI signals, obtained from the two solenoid-operated diesel injectors, are proposed. The absolute error of the correlations for determining the delay time between SoE and SoI is $\pm$ 0.05 ms, this means around 10% of the difference with the mean value of the delay time measured in all tested situations.

The model has demonstrated its ability to reproduce the rates of injection, with different solenoid operated injectors, under different situations: i) under single or split injections, ii) under different injection pressure and/or energizing time and/or iii) with different fuel properties within the range established by standards EN590 and EN15940 for diesel and GTL fuels, respectively.

Modelled and experimental results obtained show that cycle to cycle differences are lower than 1% independently of the injector model and the fuel tested. These results are acceptable for their use in thermodynamic diagnosis. However, shot to shot differences could be questionable depending on the final use of the modelled RoI, as for example in fuel spray modelling.

The use of modelled rates of injections, as input data in thermodynamic diagnosis under different engine operating modes and fuels, has similar accuracy when determining the T_i, the RoHR, and the HRL.

Summarizing, this proposed model can be a useful and alternative tool for estimating rates of injection at any operation engine mode and with any calibration thereof, without the need to carry out a test of the rate of injection. Although the differences between shot to shot are sometimes high, do not affect directly the thermodynamic diagnosis. However, the slopes could be calculated more accurately, the model could be improved in this sense in future works.

ACKNOWLEDGEMENTS

This study was carried out under the framework of the POWER Ref. ENE2014-57043-R project financed by the Spanish Ministry of Economy and Competitiveness. Authors also would like to thank the *Sostenibilidad* Program 2015-2016 of the University of Antioquia for financial support provided to Ávila. C. Authors gratefully acknowledge the companies Repsol (Spain) and Sasol (South Africa) for supplying the test fuels. Authors wish to thank the technical support provided by CMT - Motores Térmicos at Universitat Politècnica de València (Spain).

REFERENCES

[1]. Herfatmanesh MR, Lu P, Attar MA, Zhao H. Experimental investigation into the effects of two-stage injection on fuel injection quantity, combustion and emissions in a high-speed optical common rail diesel engine. Fuel Jul. 2013;109:137-147.

[2]. Xu-Guang T, Hai-Lang S, Q Tao, Zhi-Qiang F, Wen-Hui Y. The Impact of Common Rail System's Control Parameters on the Performance of High-power Diesel. 2012 International Conference on Future Energy, Environment, and Materials Energy Procedia Jan. 2012;16:2067-2072.

[3]. Payri R, López JJ, Salvador FJ, Martí Aldaraví P. Development of a methodology to learn the characteristics and performances of common rail injection systems based on simulations with AMESim. International Journal of Engineering Education Jan. 2013;29(2):533-547.

[4]. Payri R, Climent H, Salvador FJ, Favennec AG. Diesel Injection System Modelling. Methodology and Application for a First-generation Common Rail System. Proceedings of the Institution of Mechanical Engineers, Part D: Journal of Automobile Engineering Jan. 2004;218:81-91.

[5]. Seykens XLJ, Somers LMT, Baert RSG. Modelling of common rail fuel injection system and influence of fluid properties on injection process. Proceedings of VAFSEP2004, 6-9 July 2004, Dublin, Ireland. [Online]. Available, http://mate.tue.nl/mate/pdfs/4688.pdf

[6]. Chung N-H, Oh B-G, Sunwoo M-H. Modelling and injection rate estimation of common-rail injectors for direct-injection diesel engines. Proceedings of the Institution of Mechanical Engineers, Part D: Journal of Automobile Engineering Jun. 2008;222:1089-1001.

[7]. Payri R, Salvador FJ, Martí-Aldaraví P, Martínez-López J. Using one-dimensional modeling to analyse the influence of the use of biodiesels on the dynamic behavior of solenoid-operated injectors in common rail systems: Detailed injection system model. Energy Conversion and Management Feb. 2012;54:90–99.

[8]. Marčič S, Marčič M, Praunseis Z. Mathematical Model for the Injector of a Common Rail Fuel-Injection System. Engineering Jun. 2015;7:307-321.

[9]. Salvador FJ, Gimeno J, De la Morena J, Carreres M. Using one-dimensional modeling to analyze the influence of the use of biodiesels on the dynamic behavior of solenoid-operated injectors in common rail systems: Results of the simulations and discussion. Energy Conversion and Management Feb. 2012;54:122–132.

[10]. Salvador FJ, Plazas AH, Gimeno J, Carreres M. Complete modelling of a piezo actuator last-generation injector for diesel injection systems. International J of Engine Research Sep. 2014;15(1):3–19.

[11]. Plamondon E, Seers P. Development of a simplified dynamic model for a piezoelectric injector using multiple injection strategies with biodiesel/diesel-fuel blends. Applied Energy Oct. 2014;131:411–424.

[12]. Payri R, Gimeno J, Novella R, Bracho G. On the rate of injection modeling applied to direct injection compression ignition engines. International Journal of Engine Research. IMechE Mar. 2016;17(10):1015-1030.

606 [13]. Boudy F, Seers P. Impact of physical properties of biodiesel on the injection process
607 in a common-rail direct injection system. Energy Conversion and Management Dec.
608 2009;50:2905–2912.
609 [14]. Payri F, Molina S, Martín J, Armas O. Influence of measurement errors and
610 estimated parameters on combustion diagnosis. Applied Thermal Engineering Feb.
611 2006;26(2-3):226-236.
612 [15]. Hwang J, Bae C, Gupta T. Application of waste cooking oil (WCO) biodiesel in a
613 compression ignition engine. Fuel Jul. 2016;176:20–31.
614 [16]. Lapuerta M, Armas O, Bermudez V. Sensitivity of diesel engine thermodynamic
615 cycle calculation to measurement errors and estimated parameters. Applied Thermal
616 Engineering 2000;20(9):843-861.
617 [17]. Armas O, Martínez-Martínez S, Mata C, Pacheco C. Alternative method for bulk
618 modulus estimation of Diesel fuels. Fuel Mar. 2016;167:199–207.
619 [18]. Payo I, Sánchez L, Caño E, Armas O. Control Applied to a Reciprocating Internal
620 Combustion Engine Test Bench under Transient Operation: Impact on Engine
621 Performance and Pollutant Emissions. Energies Oct. 2017;10(11):1690.
622 [19]. Sajjad H, Masjuki HH, Varman M, Kalam MA, Arbab MI, Imtenan S, Ashrafur
623 Rahman SM. Engine combustion, performance and emission characteristics of gas
624 to liquid (GTL) fuels and its blends with diesel and bio-diesel. Renewable and
625 Sustainable Energy Reviews Feb. 2014;30:961-986.
626 [20]. Payri R, Salvador FJ, Gimeno J, Bracho G. The effect of temperature and pressure
627 on thermodynamic properties of diesel and biodiesel fuels. Fuel Mar.
628 2011;90:1172–1180.
629 [21]. Outcalt SL. Compressed-liquid density measurements of three alternative turbine
630 fuels. Fuel May 2014;124:1–6.
631 [22]. Rackett HG. Equation of state for saturated liquids. Journal of Chemical &
632 Engineering Data Oct. 1970;15:514.
633 [23]. Malhotra R, Dymond JH. The Tait equation: 100 years on. International Journal
634 Thermophysics Nov. 1988;9:941–51.

[24]. Payri R, Salvador FJ, Gimeno J, Bracho G. Effect of fuel properties on diesel spray development in extreme cold conditions. Proceedings IMechE Part D: J. Automobile Engineering Oct. 2008;222:1743-1753.

[25]. Kouzel B. How pressure affects liquid viscosity. Hydrocarbon Processing Petrol. Refiner 1965;44(3):120–130.

[26]. Fernández-Yáñez P, Armas O, Gómez A, Gil A. Developing computational fluid dynamics (CFD) models to evaluate available energy in exhaust systems of diesel light-duty vehicles. Applied Sciences Jun. 2017;7(6):590.

[27]. Lapuerta M, Armas O, Hernández JJ. Diagnosis of DI Diesel combustion from in-cylinder pressure signal by estimation of mean thermodynamic properties of the gas. Applied Thermal Engineering May 1999;19(5):513-529.

[28]. Catania AE, Ferrari A, Manno M, Spessa E. Experimental Investigation of Dynamics Effects on Multiple-Injection Common Rail System Performance. ASME. J. Eng. Gas Turbines Power Mar. 2008;130(3):032806.

[29]. Benajes J, Payri R, Molina S, Soare V. Investigation of the Influence of Injection Rate Shaping on the Spray Characteristics in a Diesel Common Rail System Equipped with a Piston Amplifier. ASME. Journal of Fluids Engineering Jul. 2005;127(6):1102-1110.

[30]. Cárdenas MD, Armas O, Mata C, Soto F. Performance and pollutant emissions from transient operation of a common rail diesel engine fueled with different biodiesel fuels. Fuel Dec. 2016;185:743-762.

[31]. Way RJB. Methods for the determination of composition and thermodynamic properties of combustion products for internal combustion engine calculations. Proceedings of the Institution of Mechanical Engineers Jun. 1977;190(60/76):687-697.

[32]. Armas O. "Diagnóstico Experimental del Proceso de Combustión en Motores Diésel de Inyección Directa". Ph.D. Thesis, Universidad Politécnica de Valencia. Valencia, 1999 (in Spanish). ISBN 84-7721-722-X.

NOMENCLATURE / ABBREVIATIONS

A Amps

A_o	Total injection discharge section area
B(T)	Tait parameter
C_d	Injector nozzle discharge coefficient
d_1	Time lag between SoE and SoI
d_2	Time lag between EoE and EoI
D_T	Time lag between injections
EoE	End of energizing time
EoI	End of injection time
ET	injector energizing time
Fr	Relative fuel-air ratio
$\left(\frac{f}{a}\right)_{st}$	Stoichiometric fuel-air ratio
GTL	Gas To Liquid fuel
$\mathbf{h_{finj}}$	Enthalpy of injected fuel
HRL	Heat release law
IRI	Injection rate indicator
m	Main injection
m_i	Instantaneous In-cylinder trapped mass
$\mathbf{m_b}$	Mass of stoichiometrically burnt products
$\mathbf{m_{bb}}$	Mass of blow-by
$\mathbf{m_{fev}}$	Mass of evaporated fuel
$\dot{m}_f$	Fuel mass flow rate
m_f	Total fuel mass injected
MWa	Molecular weights of air
MWb	Molecular weights burnt products
MWf	Molecular weights of fuel
NEDC	New European Driving Cycle
p	Preinjection
P0	Reference pressure
P_{rp}	Back pressure of injector fuel return
P_{back}	Back pressure inside the fuel indicator
p_i	In-cylinder gas pressure
P_{inj}	Injection pressure
ρ_f	Fuel density

699	$\boldsymbol{Q_w}$	Heat transferred to cylinder walls
700	**Ra**	Specific air constant
701	**Rb**	Specific constant of burnt products
702	$\boldsymbol{R_i}$	Instantaneous specific constant of the In-cylinder gas
703	$\boldsymbol{R_e}$	Reynolds number
704	**Rf**	Specific constant of the evaporated fuel
705	**Rμ**	Universal constant
706	**RoHR**	Rate of heat release
707	**RoI**	Rate of fuel injection
708	**SoE**	start of injector energizing
709	**SoI**	Start of injection
710	**T0**	Reference temperature
711	**TRI**	Triangulate model of the rate of injection
712	$\boldsymbol{T_i}$	Instantaneous in-cylinder mean gas temperature
713	$\boldsymbol{t_{iny}}$	Fuel injection duration
714	$\boldsymbol{u_a}$	Internal energy of air
715	$\mathbf{u}_i$	Internal energy in-cylinder trapped mass
716	$\mathbf{u}_b$	Internal energy of stoichiometrically burnt products
717	$\boldsymbol{u_f}$	Internal energy of fuel
718	$\boldsymbol{\mu_f}$	Fuel dynamic viscosity
719	**V**	Volts
720	$\boldsymbol{V_i}$	In-cylinder calculated volume
721	$\boldsymbol{v_f}$	Fuel kinematic viscosity
722	$\mathbf{Y}_{xi}$	Mass fractions
723	$\mathbf{Y_b}$	Stoichiometrically mass fraction burnt products
724	**0D**	Zero-dimensional model
725	**1D**	One dimensional model
726		

Figures

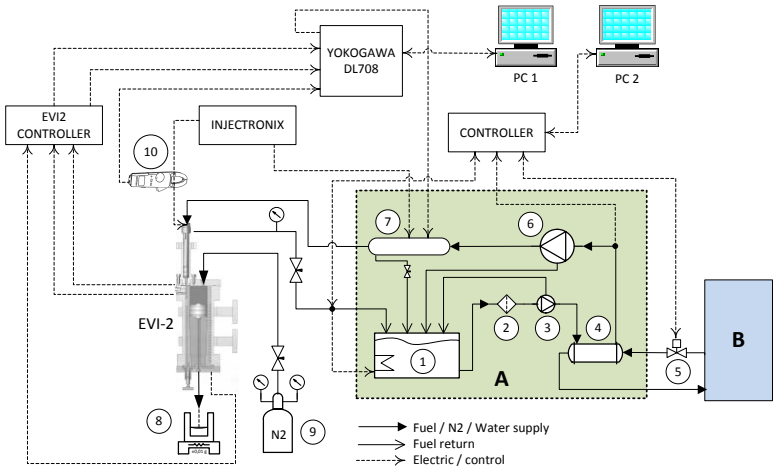

- **A:** Bench BOSCH® EPS 711.
- **B:** Water chiller EUROKLIMAT® IP20.
- **PC1:** YOKOGAWA DL708 computer
- **PC2:** Control and measure Injection rate computer
- **1:** Fuel tank
- **2:** Fuel filter
- **3:** Low pressure pump
- **4:** Heat exchanger
- **5:** Solenoid valve
- **6:** High pressure pump CP1
- **7:** Common-rail
- **8:** Precision balance Kern PFB
- **9:** N2 supply and pressure regulator
- **10:** Current clamp Hantek CC65

Figure 1. Simple functional scheme experimental installation.

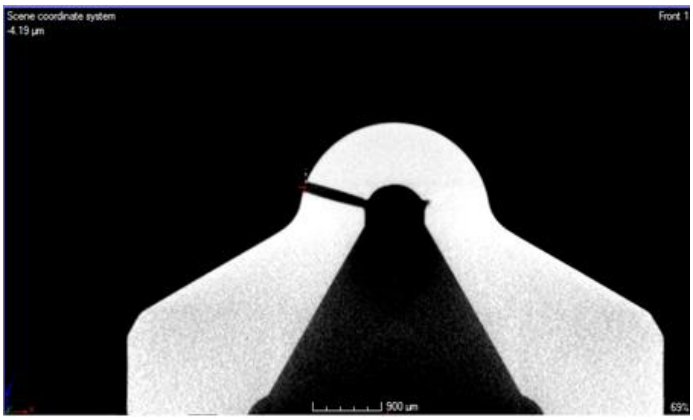

Figure 2. Example of image from the tip of injector obtained by means X-ray analysis.

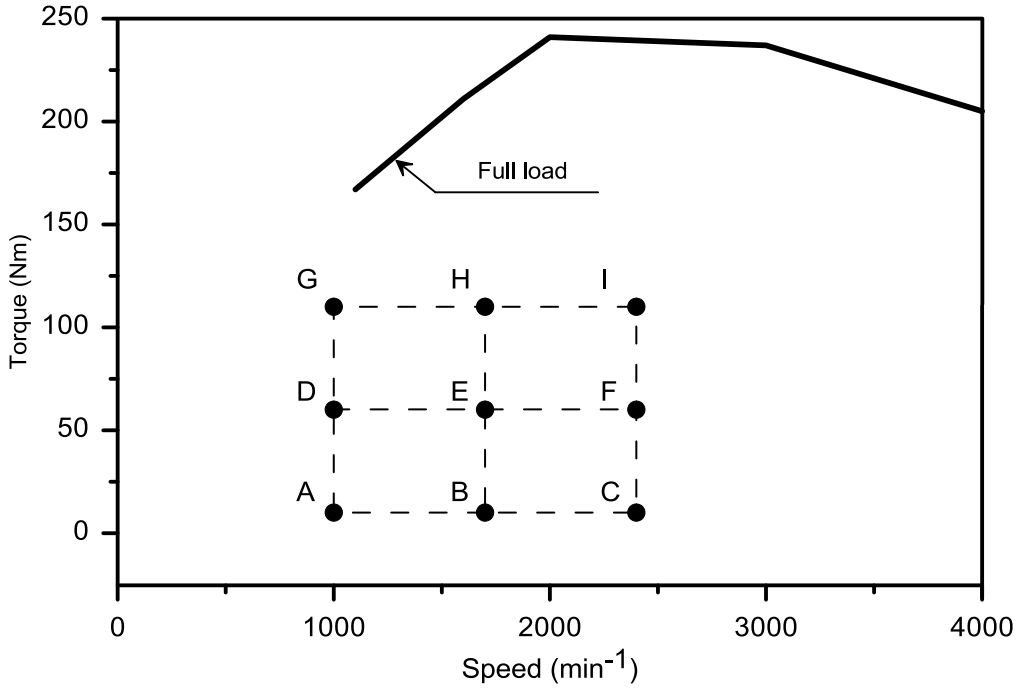

Figure 3. Engine operating modes used for 0D model input data with 7H150 injector.

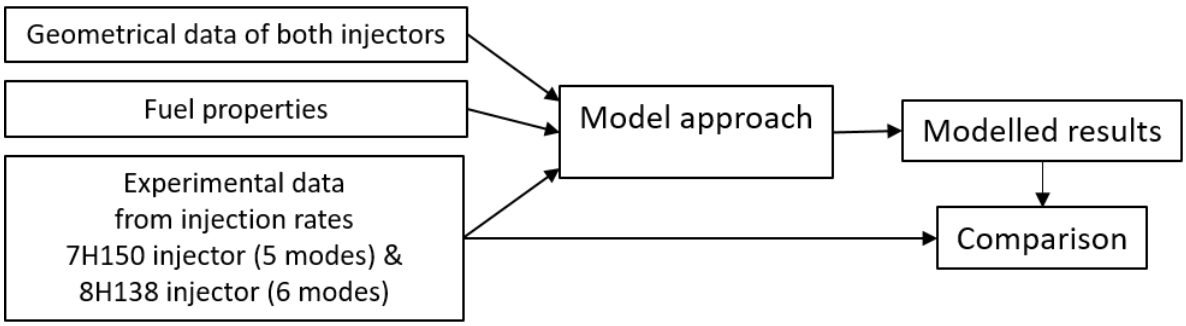

Figure 4 Methodology for model approach.

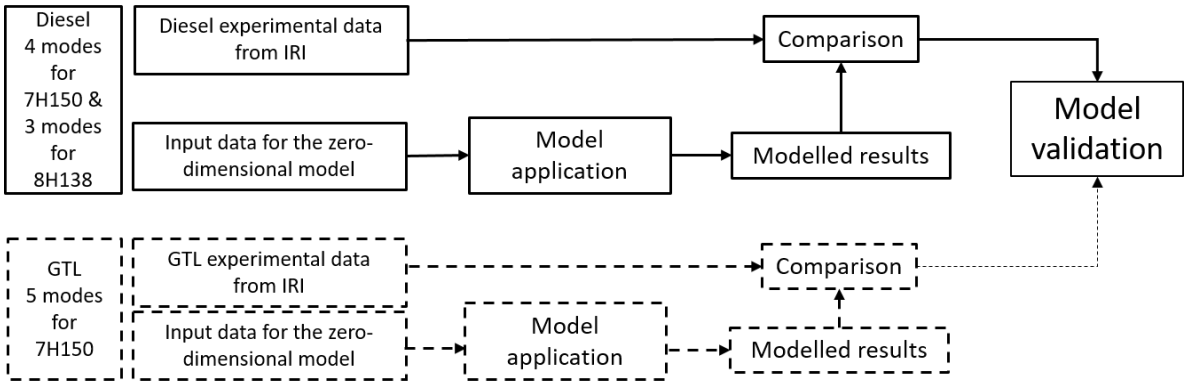

Figure 5 Methodology for model approach and its validation with different fuels.

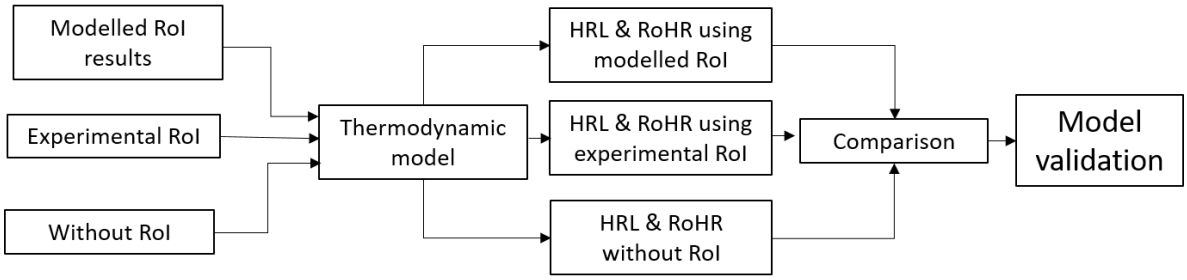

Figure 6 Methodology to compare thermodynamic diagnosis results.

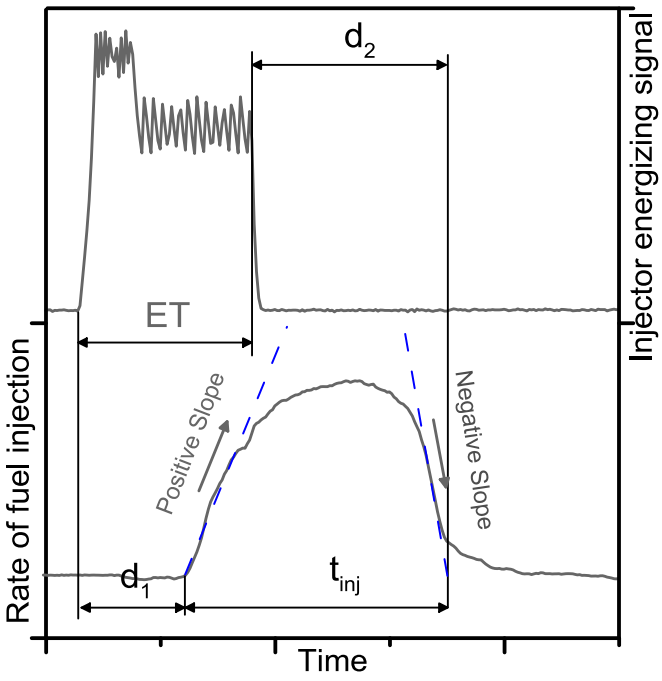

Figure 7. Experimental actual event of fuel injection process.

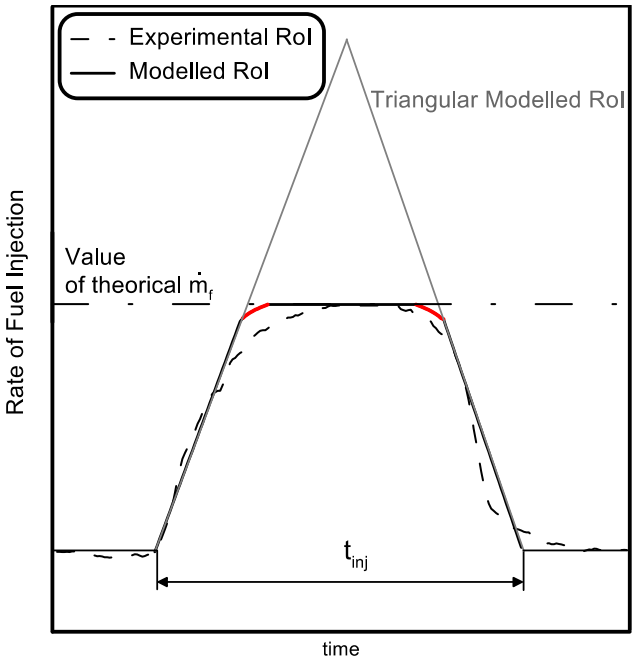

Figure 8. Simple modelled rates of fuel injection vs experimental rate.

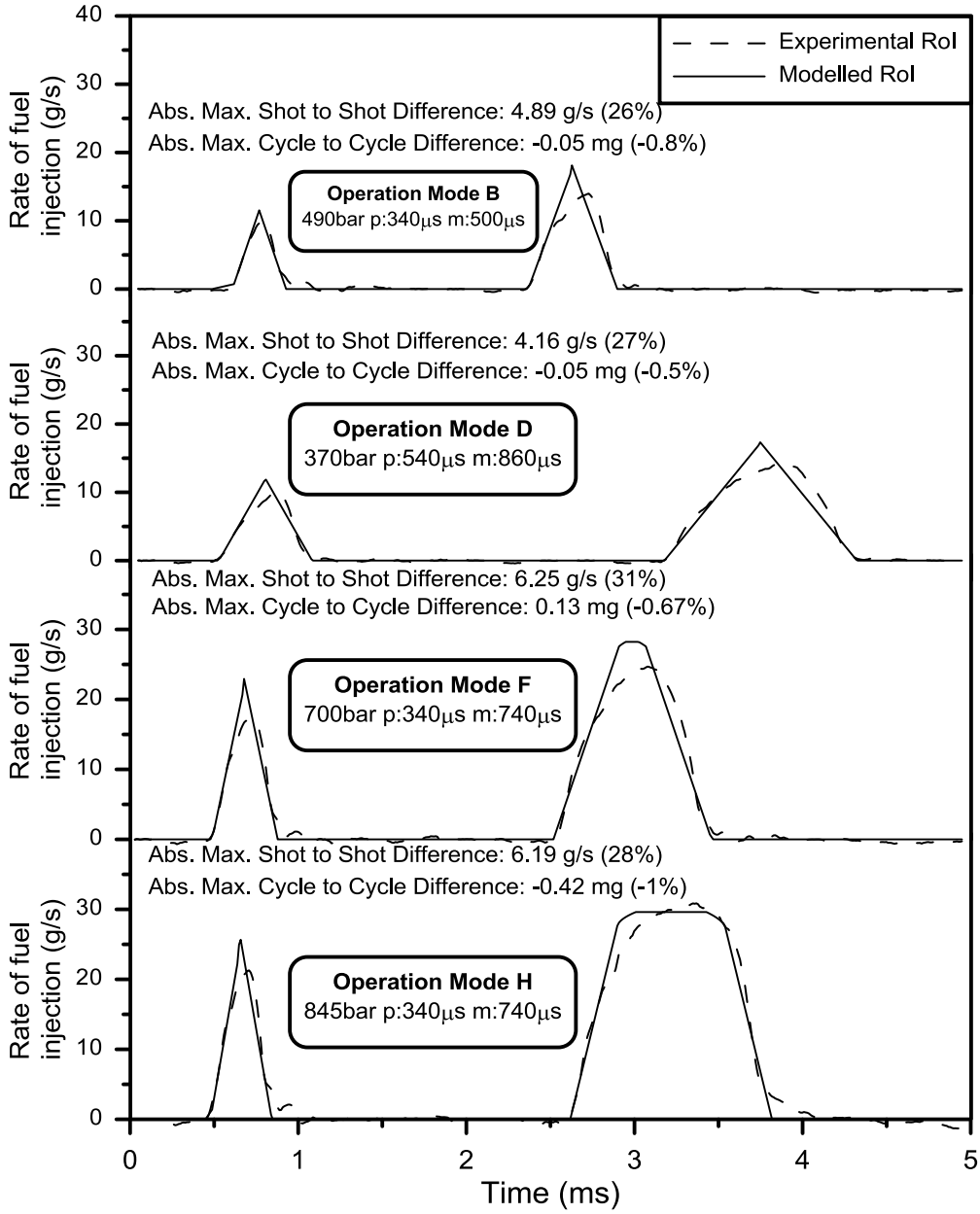

Figure 9. Modelled and experimental rates of injection. Operating modes B, D, F and H, were used for model validation.

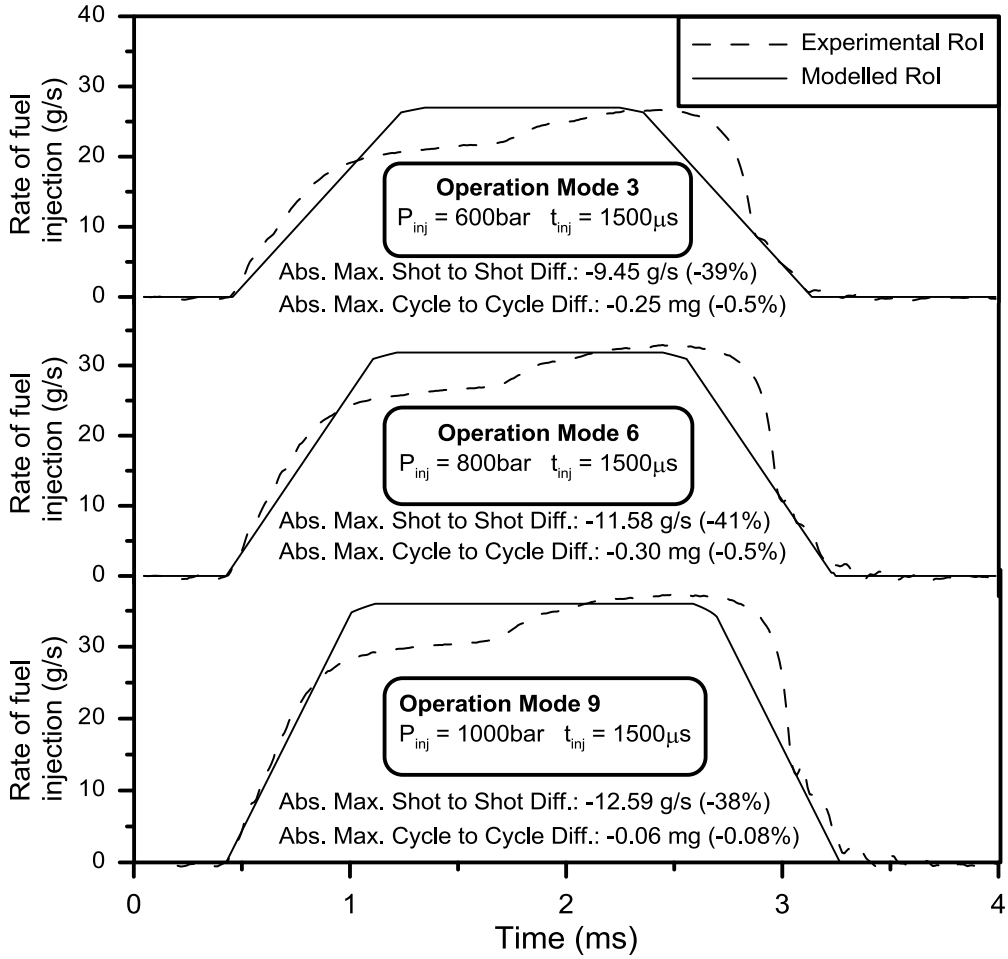

Figure 10. Modelled and experimental rates of injection. Operating modes 3, 6 and 9, used for model validation of the injector 8H138.

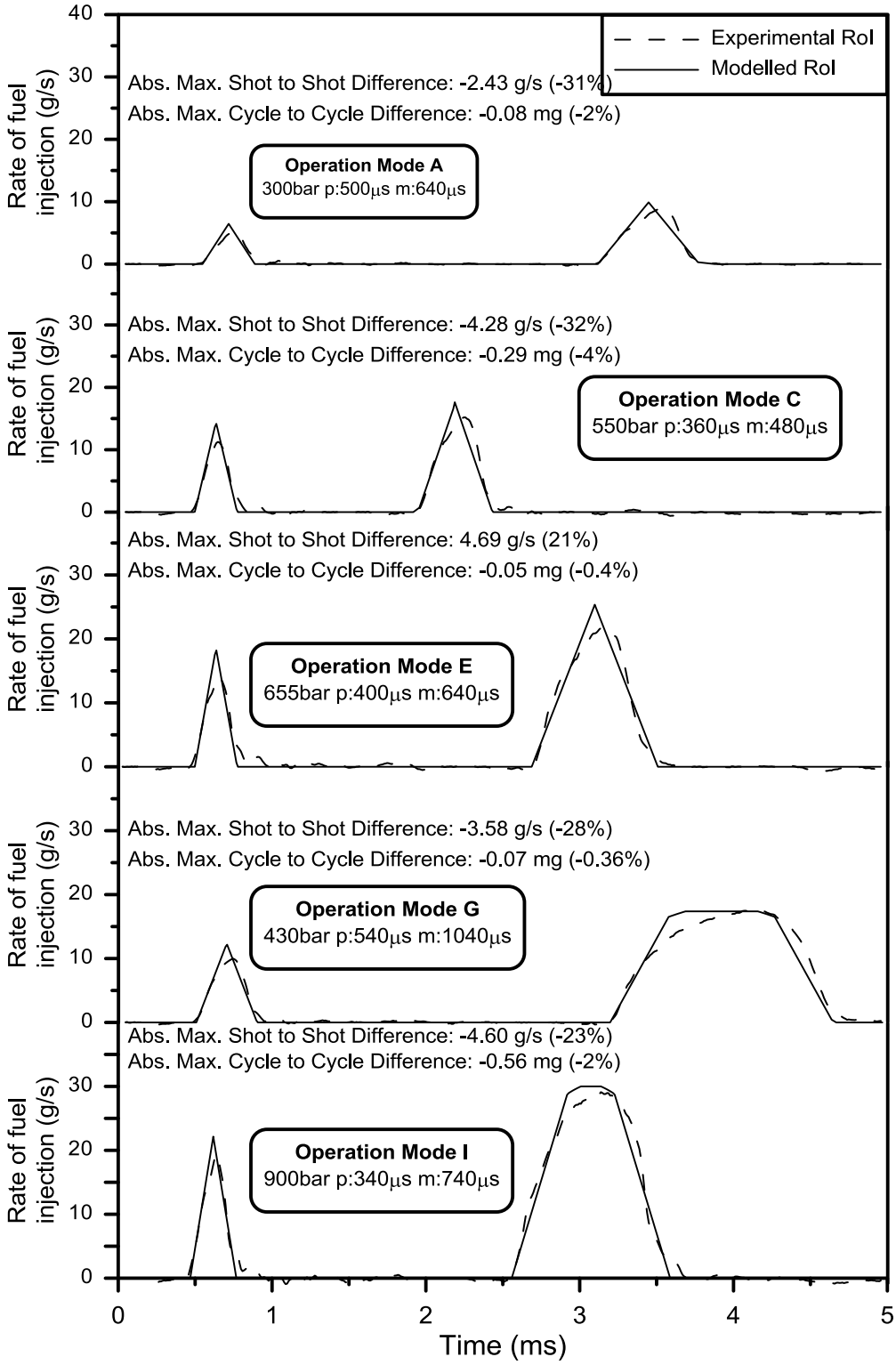

Figure 11. Modelled and experimental rates of injection. Operating modes A, E and I, used for model approach and GTL fuel.

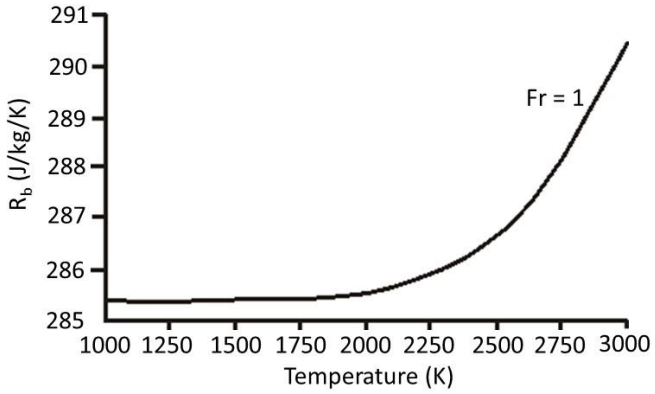

Figure 12. Variation of the specific constant of stoichiometric burnt products [31]

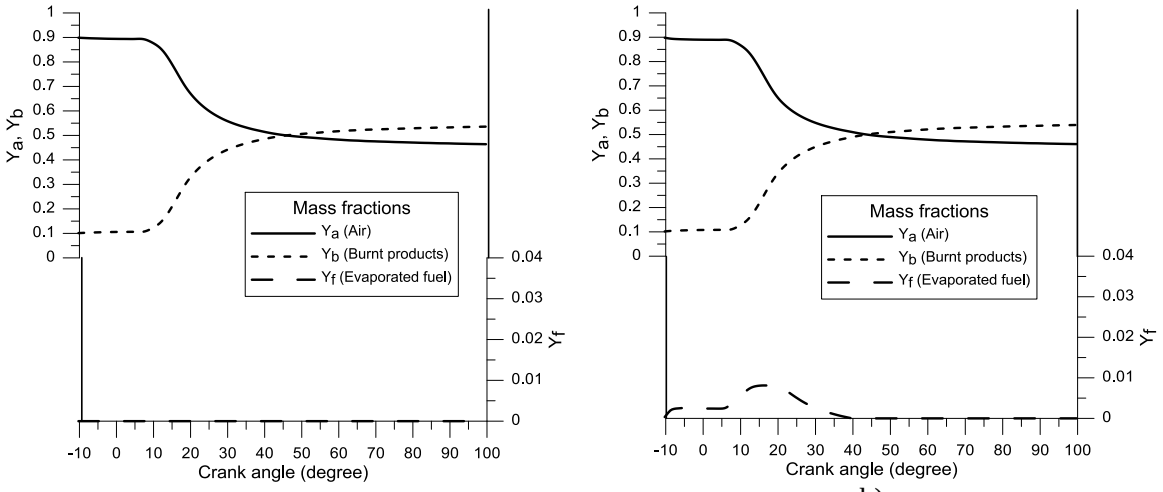

Figure 13. Evolution of the air, evaporated fuel and stoichiometric burnt products mass fractions a) under a combustion engine without rate of fuel injection & b) under a combustion engine with a split rate of fuel injection.

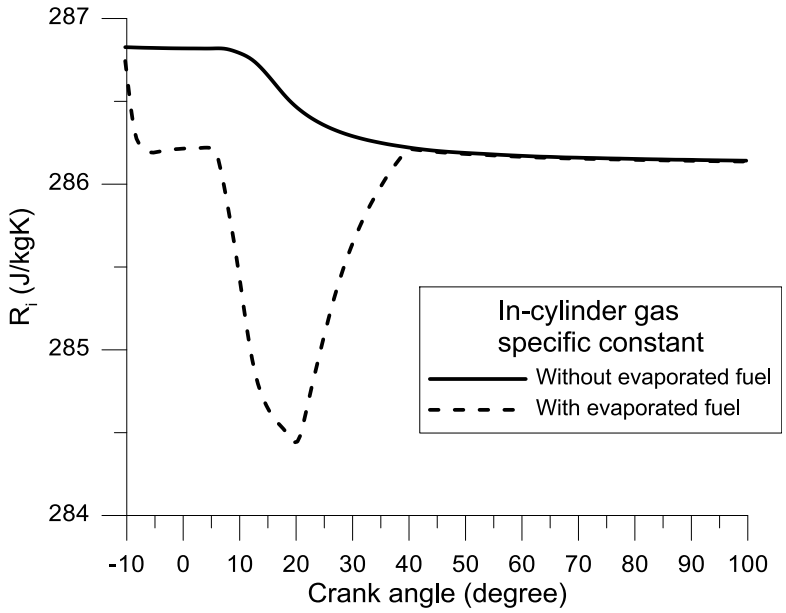

Figure 14 Evolution specific constant of the in-cylinder gas with split injection.

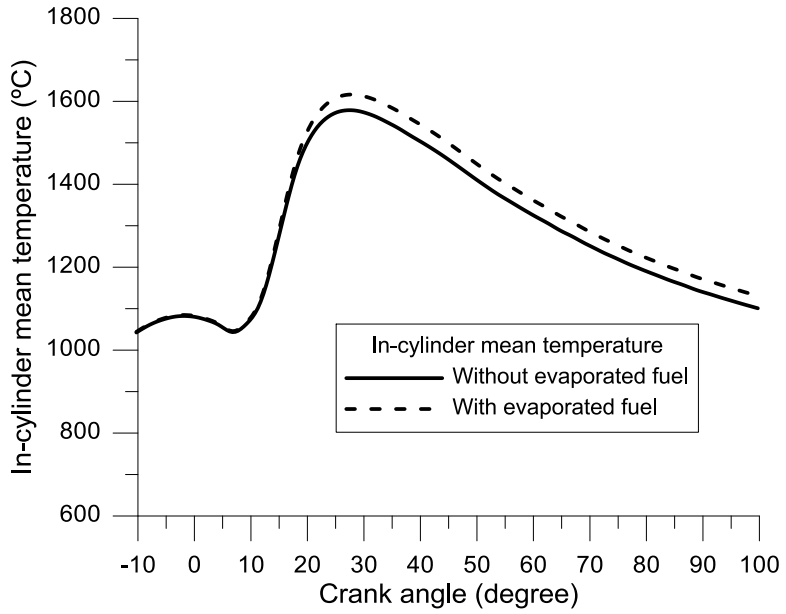

Figure 15 Evolution of mean temperature In-cylinder gas with split injection.

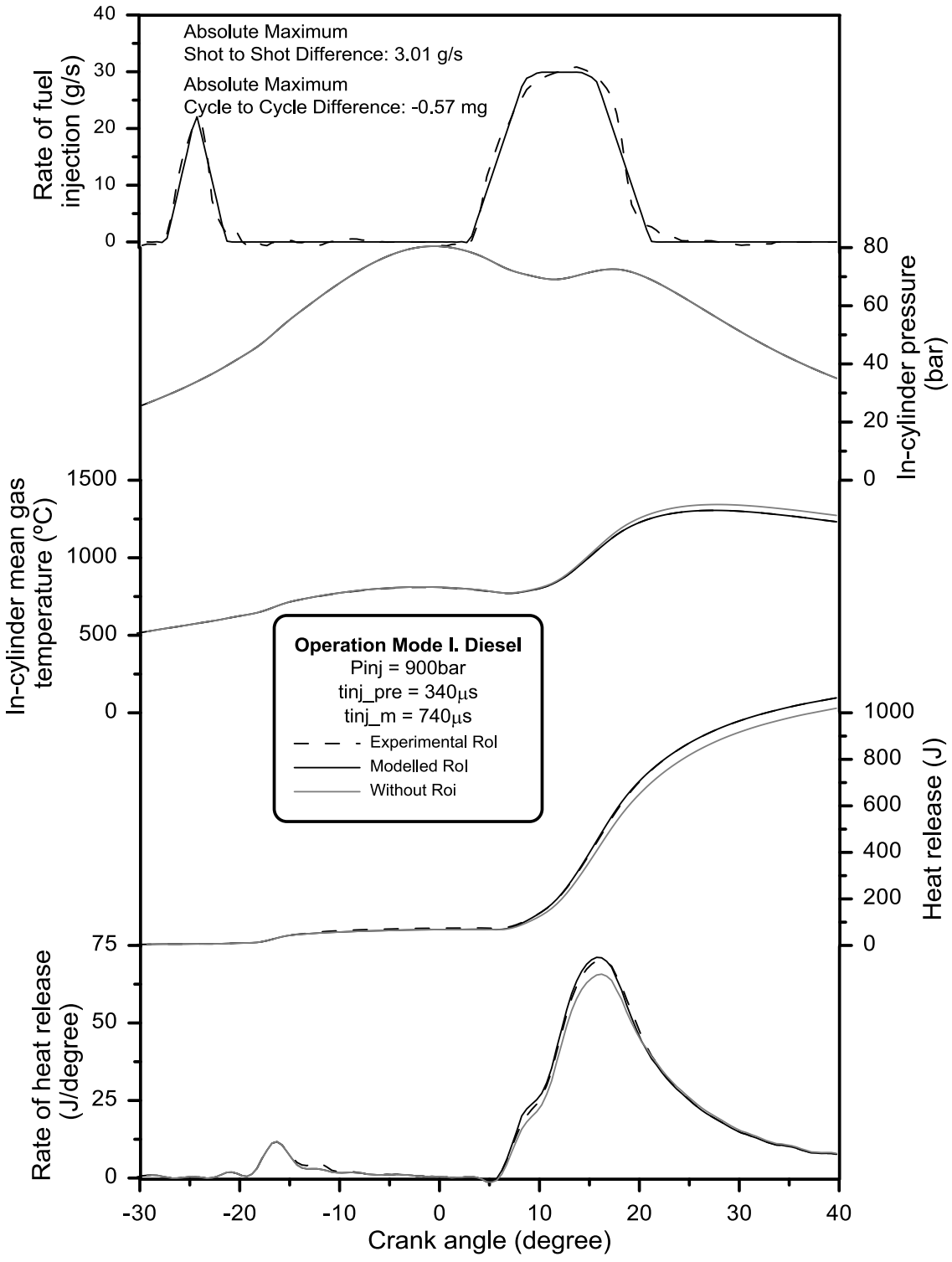

Figure 16. Thermodynamic diagnosis of the combustion process with diesel fuel from operating mode I.

Tables

Table 1. Engine characteristics.

Type	Nissan YD22, 2.184 l, turbocharged + intercooler
Fuel injection	Common rail, pilot injection
Maximum power	82kW at 4000min^{-1}
Maximum torque	248Nm at 2000min^{-1}
Cylinder arrangement	4 cylinders, in line
Bore/stroke	86.5/94mm
Compression ratio	16.7:1

Table 2. Fuel properties.

Properties	*diesel*	*GTL*
Molecular Formula	$C_{15.18}H_{29.13}$	$C_{16.89}H_{35.77}$
Molecular weight (g/mol)	211.4	238.6
H/C Ratio	1.92	2.12
Stoichiometric fuel–air ratio	1/14.64	1/14.95
Low heating value (MJ/kg)	42.43	43.86
Cold filter plugging point (ºC)	-17	-7
Lubricity (WS1.4) (µm)	333	330
Cetane number	54.2	73

Table 3. Kinematic viscosity and density of fuels tested at different temperatures with atmospheric pressure.

Temperature (ºC)	υ_f *at Patm (cSt)*		μ_f *at Patm (cPo)*		ρ_f *at Patm (kg/m^3)*	
	diesel	*GTL*	*diesel*	*GTL*	*diesel*	*GTL*
15	5.24	4.66	4.43	3.60	845	773.5
25	4.64	3.91	3.90	3.00	840	767
40	3.55	2.97	2.94	2.25	827	757.5

Table 4. Main characteristic parameters of injection for split injection with Denso 7H150 injector (9 engine modes).

Mode	Engine speed (min^{-1}) - Torque (Nm)	Injection pressure (bar)	ET (μs)		Dwell (μs)	P_{back} (bar)
			Pre injection	Main injection		
A*	1000 – 10	300	500	640	2085/2585	60
B	1700 – 10	490	340	500	2130/2670	
C*	2400 – 10	550	360	480	2130/2670	
D	1000 – 60	370	540	860	1425/1765	
E*	1700 – 60	655	400	640	1100/1460	
F	2400 – 60	700	340	740	1855/2255	
G*	1000 – 110	430	540	1040	1655/2015	
H	1700 – 110	845	340	740	2015/2355	
I*	2400 – 110	900	340	740	1815/2155	

* Modes used to model approach

Table 5. Main injection characteristic parameters for single injection using Denso 8H138 injector.

Mode	Injection pressure (bar)	Energizing time (μs)	P_{back} (bar)
1*	600	500	80
2*		1000	
3		1500	
4*	800	500	95
5*		1000	
6		1500	
7*	1000	500	90
8*		1000	
9		1500	

* Modes used to model approach

Table 6. Coefficients of d_1 and d_2 correlations.

Coefficients	*Values for d1*	*P-value*	*Coefficients*	*Values for d2*	*P-value*
a_1	1.02565	0.0000	b_1	0.60913	0.0000
a_2	-0.00420	0.0000	b_2	0.01194	0.0000
a_3	0.00327	0.0000	b_3	-0.03598	0.0000
a_4	-0.07541	0.0000	b_4	0.89404	0.0000
a_5	0.00632	0.0002	-	-	-

Table 7. Coefficients of correlation for determination of positive and negative slope.

Coefficients	*Value Slope*	*P-value*
c_1	2.2205	0.0000
c_2	-0.0513	0.0000
c_3	-0.0894	0.0000